Decoration of silicon nanowires with silver nanoparticles for ultrasensitive surface enhanced Raman scattering

Cristiano D'Andrea[1,9], Maria J Lo Faro[1,2,3,9], Giulia Bertino[3], Paolo M Ossi[4], Fortunato Neri[5], Sebastiano Trusso[2], Paolo Musumeci[3], Matteo Galli[6], Nicola Cioffi[7], Alessia Irrera[2], Francesco Priolo[1,3,8] and Barbara Fazio[2]

[1] MATIS IMM—CNR, Via Santa Sofia 64, I-95123 Catania, Italy
[2] IPCF—CNR, V.le F. Stagno d'Alcontres 37, I-98156 Messina, Italy
[3] Dipartimento di Fisica ed Astronomia, Università di Catania, Via Santa Sofia 64, I-95123 Catania, Italy
[4] Dipartimento di Energia, Center for Nanoengineered Materials and Surfaces-NEMAS, Politecnico di Milano, via Ponzio 34-3, I-20133 Milano, Italy
[5] Dipartimento di Scienze Matematiche e Informatiche, Scienze Fisiche e della Terra, Università di Messina, V.le F. Stagno d'Alcontres, 31, 98166, Messina, Italy
[6] Dipartimento di Fisica, Università degli Studi di Pavia, via Bassi 6, 27100 Pavia, Italy
[7] Dipartimento di Chimica, Università degli Studi Bari 'Aldo Moro', Via E. Orabona 4, 70126 Bari, Italy
[8] Scuola Superiore di Catania, Via Valdisavoia 9, I-95123 Catania, Italy

Silicon nanowires (Si NWs), produced by the chemical etching technique, were decorated with silver nanoparticles (NPs) produced at room temperature by the pulsed laser deposition (PLD) technique. Silver NPs were obtained by means of nanosecond pulsed laser ablation of a target in the presence of a controlled Ar atmosphere. Two different laser pulse numbers and Si NWs having different lengths were used to change the NP number density on the Si NW surface. The resulting Ag NP morphologies were studied by scanning electron microscopy imaging. The results show that this industrially compatible technological approach allows the coverage of the Si NW walls with Ag NPs with a strong control of the NP size distribution and spatial arrangement. The obtained Ag NP decorated Si NWs are free from chemicals contamination and there is no need of post deposition high temperature processes. The optical properties of Si NW arrays were investigated by reflectance spectroscopy that showed the presence of a plasmon related absorption peak, whose position and width is dependent on the Ag NP surface morphology. Coupling the huge surface-to-volume ratio of Si NW arrays with the plasmonic properties of silver nanoparticles resulted in a 3D structure suitable for very sensitive surface enhanced Raman scattering (SERS) applications, as demonstrated by the detection of Rhodamine 6G in aqueous solution at a concentration level of 10−8 M. Keywords: silicon nanowires, pulsed laser ablation, silver nanoparticles, SERS (Some figures may appear in colour only in the online journal)

E-mail: trusso@me.cnr.it and irrera@me.cnr.it

Received 27 April 2016, revised 17 June 2016
Accepted for publication 22 June 2016
Published 9 August 2016

1. Introduction

Silicon nanowires (Si NWs) strongly attract worldwide research interest for their unique and advantageous properties arising from confinement in two directions. Both the electrical

and optical properties are dramatically modified with respect to the bulk material, which makes them suitable candidates to become the building blocks for applications in future electronic devices [1, 2], photovoltaic cells [3, 4], sensors [5, 6] and light emitting devices [7, 8]. The most adopted bottom-up approach is the vapor–solid–liquid (VLS) technique. However, it is affected by heavy drawbacks, such as poor control of the doping level, which is a strongly detrimental aspect for Si NW applications, and the presence of a metallic catalyst in the NWs [9], which limits the optical and electrical performances of the system. In contrast, the metal assisted chemical etching (MACE) approach is a rapid and low cost technique, which allows uniform Si NWs fabrication [10–15]. In particular, the process can be performed with inexpensive systems and at room temperature. Therefore, the resulting NWs are not affected by metal diffusion and deep impurity levels, which commonly result in undesired non-radiative recombination, and the doping is the same as that of the initial substrate. Thus, the final Si NW dense forest structure offers a wide range of possibilities for further implementations. Many groups have decorated Si NW arrays with metal nanoclusters for different applications [16–21].

In general, silver and gold are the most used metals, due to their interesting behaviors at the nanosize. When the particle size of metals like gold or silver reduce to the nanometric scale, in fact, peculiar optical properties arise that are absent in their bulk counterparts, driven by the presence of free conduction electrons. In particular, when the size of the nanoparticles (NPs) is smaller than the wavelength λ of an external electromagnetic (EM) field, all the conduction electrons of the NPs are subjected to the same homogenous EM field and oscillate collectively. The collective motion of the electrons behaves as an oscillating dipole that will be in resonance at a given frequency of the external EM field, giving rise to a maximum in the absorption. Such a phenomenon is known as surface plasmon resonance (SPR). When the external EM field is in resonance with the SPR absorption peak, the EM field in correspondence wiith sharp structures or gaps on the nanostructured surface can be enhanced by several order of magnitude and so the Raman intensity scattered by a molecule adsorbed at such sites. Most of the plasmonic substrates employed in SERS application are made of gold and silver. The relative SPR position, in fact, lies in the visible portion of the EM spectrum allowing the coupling of the SPR with the excitation wavelength used in Raman spectroscopy. The Raman enhancement of silver is higher than the one of gold, but the latter is more stable and biologically friendly, nevertheless Ag NP coated substrates can still be used in biological applications when properly functionalized to capture complex biological system like DNA [22].

Concerning the decoration of Si NWs with both silver and gold NPs, chemical routes are the most adopted approaches, even if they do not allow fine control of the NP growth processes and hence on the structural characteristics of metal clusters [17–21]. Moreover metal clusters are surrounded by a chemical shell that limits the applications of such systems [16–19]. In some cases the reduction of the Si NW diameter was reported after the chemical growth of Ag NPs, thus limiting the Ag NP deposition time [23]. Chemical reduction methods were adopted, also, to decorate an ordered treelike Si/ZnO system for SERS applications, but in this case the two step growth of the 3D pattern adopted, i.e. photolithography patterning and atomic layer deposition for the Si pillars and the ZnO dendrites respectively, is more costly and time expensive than the MACE process. Several papers reporting the metal decoration describe the galvanic reduction of metal ions from a solution on the Si NW surface [21]. This approach leads to the formation of metal NPs, still with poor control of their size and shape. Moreover, complete NW coverage is very difficult and occurs only on the top of the NW arrays [16–21], limiting the performance of the system. In spite of this, the realization of Si NW decoration by physical methods is still scarcely investigated. As an example, Malazimoglu *et al* [24] report the decoration of Si NWs through the evaporation of a thin Ag film and its subsequent annealing at 600 °C for 1 h. Such an approach is not compatible with Si technology owing to the high temperature needed to induce the clustering process of the evaporated Ag film.

Recently, we developed a method for the production of noble metal NP arrays by means of pulsed laser deposition (PLD) in the presence of a controlled inert atmosphere [25, 26]. The technique is based on focusing a high energy pulsed laser on the surface of a target material, the laser pulse induces the vaporization of a portion of the irradiated area. In the so formed high-density plasma cloud a large amounts of NPs sized in the few nanometers range are formed owing to the interaction with the ambient gas [27, 28]. By properly selecting the values of a set of experimental parameters, such as laser fluence, gas nature and pressure, number of laser pulses and target to substrate distance, fine control of NP dimension and spatial arrangement on the substrate surface can be achieved. In previous work, we demonstrated that on flat substrates both silver and gold nanostructured thin films can be grown with different surface morphologies. Surface morphologies characterized by the presence of isolated nearly spherical NPs, nano-sized islands with smooth edges, nearly and fully percolated structures can be obtained by changing two easily accessible parameters, namely Ar pressure and laser shots number, while keeping all the other relevant parameters fixed, i.e. laser fluence, target to substrate distance, area of the laser spot on the target surface. The nanostructured thin film formation can be synthesized as a two-step growth mechanism. In the high-density laser generated plasma cloud, a large amounts of NPs sized in the few nanometers range are formed owing to the interaction with the high pressure ambient gas [24, 25]. The so formed NPs land on the substrate surface where the the second step of the film growth takes place. Film formation, in fact, proceeds via coalescence of the deposited NPs. While the Ar pressure and the energy of the expanding plasma determine the dimension of the in flight generated NPs, the total duration of the deposition process leads to the final surface morphology [29]. Such nanostructured surfaces are characterized by the presence of localized surface plasmons (LSP) whose position and

width depend on the NP dimensions and their mutual spatial arrangements [30], showing remarkable surface enhanced Raman scattering (SERS) activity. Moreover, the fact that the growth is performed at room temperature and in the presence of an inert gas atmosphere, means issues related to annealing processes, like the one needed to grow a uniform layer of silver NPs at the end of the etching process [31] and chemical contaminations, are overcome.

In this paper, we report on the decoration of Si NWs with silver NPs by using PLD to decorate the Si NWs. The so obtained Si NWs decorated by Ag NPs are free from any chemical shell and uniform in coverage of NW length, therefore very interesting for different applications.

In particular the SERS activity of the Ag NP decorated Si NWs was tested against the presence in aqueous solution of a probe molecule (Rhodamine 6G) at different concentration levels. The influence of two parameters, namely the Si NW length and the Ag NP size and number density, controlled through the laser pulse number, on the structural properties of the substrates, and hence on their SERS activity is reported. The combination of the Si NW's huge surface to volume ratio together with the ability to control the plasmonic properties of the Ag NPs by means of easily accessible experimental parameters (Si NW length and Ag NP surface number density) demonstrate the great potential of this method.

2. Materials and methods

2.1. Silicon nanowire fabrication

Si NWs are grown on 100 oriented crystalline p-type Si substrates (commercial wafer from Siegert Wafer GmbH with a thickness of 500 μm) by silver salts metal assisted chemical etching. Si wafers are cut in 2.5 $\times$ 2.5 cm^2 pieces and an oxygen free surface is obtained, processing the samples with 2 min of UV ozone cleaning and 5 min of chemical etching in a 5% hydrofluoridric (HF) (Sigma-Aldrich, $\geqslant$99.0%) water solution. The clean substrates are immersed in the etching solution made of $AgNO_3$ (Sharlau 0.05 M) 40%, H_2O (Milli-Q Deionized water 18Mohm cm) 40% and HF 20%. Each step of Si NW growth is performed in a clean room maintained at a temperature of 20 °C (figure 1(a)). During the process silver salts dissolve in the solution leading to the formation and precipitation of small Ag clusters that act as metallic precursors for the Si NW synthesis. Due to the difference of electronegativity at the Ag/Si interface an anodic reaction occurs, producing a thin layer of silicon dioxide only underneath the metal covered regions selectively etched by HF, causing the metal NPs to sink into the Si bulk layer to form NWs. During the synthesis the formation of an overlaying silver dendrites network occurs. Silver dendrites [13] and any silver contamination can be easily removed by a quick chemical etching in pure HNO_3 (Sigma-Aldrich ACS reagent grade, 70%) solution for 10 min. We prepared Si nanowires 1.7 μm and 3.4 μm long during an etching time of

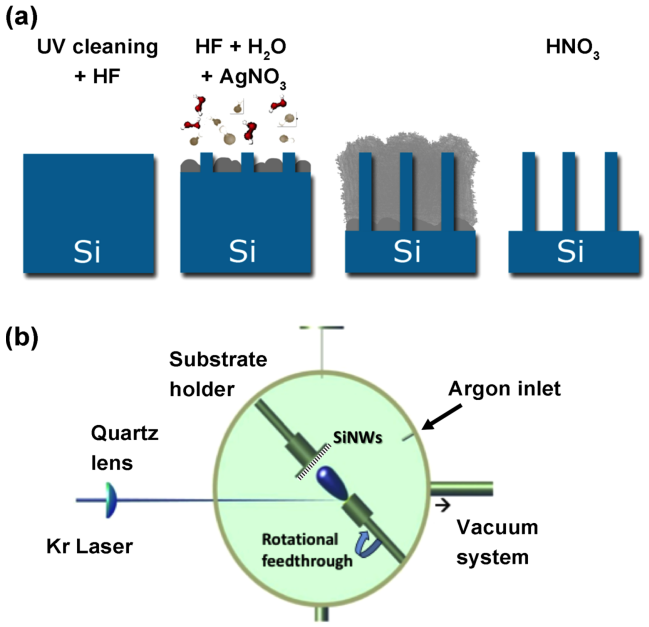

Figure 1. (a) Schematic of Si NWs fabrication by the metal assisted chemical etching process. (b) Setup of the PLD apparatus used to decorate the Si NWs.

11 min and 25 min, respectively, with all the other preparation conditions fixed.

2.2. Silver nanoparticle decoration

Decoration of the Si NWs is realized by PLD of Ag NPs. The process is realized in a high vacuum chamber with a residual base pressure of 10^{-4} Pa. The laser beam from a KrF excimer laser (Lambda Physik CompEx 205, 25 ns pulse width, 248 nm wavelength, 10 Hz repetition rate, laser fluence set at 2.0 Jcm^{-2}) is focused onto the surface of a pure silver target using a quartz lens with the silver target mounted on a rotating holder in order to avoid excessive surface damaging. Si NW samples are positioned 35 mm from the target surface and the deposition process is performed in the presence of 70 Pa of Ar. The schematic of the PLD setup is shown in figure 1(b). Under the selected deposition conditions the plasma expands through the ambient gas forming a shock wave [32], at the interface between the plasma and the ambient gas density and pressure conditions favor the in flight formation of silver clusters that subsequently land onto the substrate surfaces. The number density of the Ag NPs can be controlled by the laser pulse number [26]. In this work we adopted two different laser pulse numbers, 45 000 and 60 000, in order to realize decorated Si NWs with different surface morphologies.

2.3. Properties characterization

NW structural characterization is performed by a Scanning Electron Field Emission Zeiss Supra 25 Microscope (SEM) and a transmission electron microscope (TEM) FEI Tecnai 12 instrument. A detailed NP sizing and counting procedure is

performed using the Gatan Digital Microscopy suite software. The sizes of the Ag NPs on the NWs are obtained by a detailed structural analysis using high magnification SEM images. In figure 3(a) a cross section SEM image of sample **1** is reported. In figures 4(b)–(d) high magnification SEM cross images of three different sections of the wires are visible, respectively acquired at the top (b), center (c) and bottom part (d) of the decorated NWs. Here, the NP distributions have been calculated for each different section. The NP detailed analysis has been performed by using Gatan Digital Microscopy suite software analysis on high magnification cross-section SEM images for each section of the wire, as displayed in figures 4(b)–(d). The Ag NPs have been identified and selected by the software by adjusting the image contrast on a 350kX magnification SEM image. For each section we investigated a total area of approximately $600 \times 600\,\text{nm}^2$ to acquire a significant statistical ensemble of particles. The mean radius of Ag NPs has been evaluated by the software to calculate the radius of NPs and the radius statistics have been later analyzed by OriginLab data software analysis. The frequency counts on the particle radii have been fitted with a Gaussian function. The same procedure was adopted to analyze each section and histogram plots and fit results are reported in figures 4(e)–(g) and table 2. The interparticle distances have been measured connecting first neighbor NPs through linear segments manually drawn on the SEM image by using image processing software. The segment lengths have been counted by Gatan Digital Microscopy software and the interparticles distance statistics analyzed by using the same procedure described above.

Reflectance measurements are acquired in the range between 200–1800 nm by means of a double-beam spectrophotometer (Varian, CARY 6000i) equipped with an integrating sphere and acquired through a phototube detector in the visible range (200–800 nm) and a InGaAs photodiode in the near-infrared. Micro-Raman and SERS measurements are performed focusing an Ar^+ laser beam, tuned at 514 nm, onto the NW samples through a 50X LWD objective (NA = 0.5), with power not exceeding 510 μW (measured on the sample surface). The backscattered radiation is analysed by means of an HR800 Micro-Raman Spectrometer (Horiba) equipped with a Peltier cooled CCD (Synapse) detector. Rhodamine 6G (Carlo Erba, powder) is selected as a probe molecule for SERS measurements.

To study in detail the SERS response we prepared four samples of $2.5 \times 2.5\,\text{cm}^2$ organized in two length sets (1.7 μm and 3.4 μm), each one divided in two decoration subsets of 45 000 and 60 000 laser pulses. Each substrate has been sectioned in smaller portion of $0.5 \times 0.5\,\text{cm}^2$, that are soaked for 150 min in R6G water solutions at six different concentrations levels, ranging from 10^{-4} to 10^{-9} M, then dried in air for 2 h.

Ten spectra are acquired at different positions on the substrate surfaces, the resulting averaged spectra have been normalized for the exposure time, laser power and the fluorescence background subtracted.

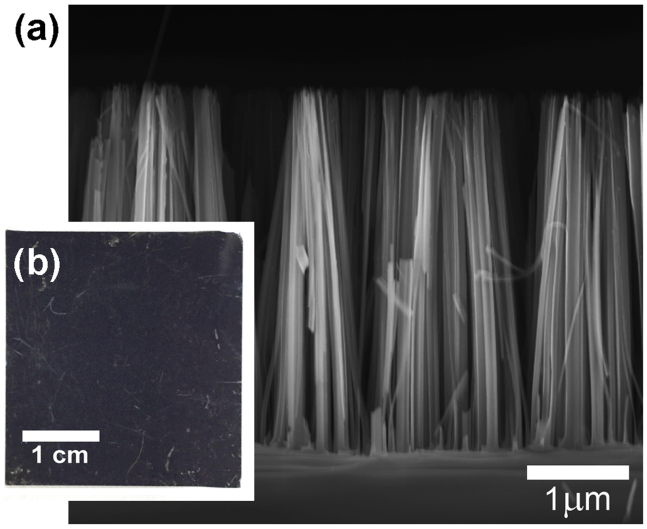

Figure 2. (a) Cross section SEM of the Si NW template of 3.4 μm realized by metal assisted chemical etching. (b) Photograph of the top surface of the Si NW sample.

Table 1. Characteristics of the Ag decorated NW samples.

Name	NW lengths	PLD shots
Sample 1	1.7 μm	45 000
Sample 2	1.7 μm	60 000
Sample 3	3.4 μm	45 000
Sample 4	3.4 μm	60 000

3. Results and discussion

3.1. Structural properties

We prepared Si NWs 1.7 μm and 3.4 μm long, depending on the etching conditions and time. As an example figure 2(a) displays a vertically and uniformly aligned array of Si NWs having a length of 3.4 μm. For simplicity we named sample **1** and sample **2** the Si NWs with the shorter length (1.7 μm) and samples **3** and **4** those that were 3.4 μm long, respectively decorated with Ag NPs by using 45 000 (**1** and **3**) and 60 000 (**2** and **4**) PLD shots (see table 1).

The structural properties of NWs covered by Ag NPs have been investigated by SEM analysis both in plan view and in cross section. All the samples showed the presence of Ag NPs along the NWs. As an example, figures 3(a) and (b) display a comparison between the plan view SEM images for sample **4** before and after the decoration process: the presence of the Ag NPs on the surface of the Si NWs can be clearly seen.

Moreover, it is worth noticing that the Si NW array is not damaged by the PLD deposition. Looking at the SEM images it can be seen that size and number density of the Ag NPs deposited along the length of the Si NWs are different when the Si NW length and laser pulse number are considered. In order to gain information about the size and spatial distribution of the Ag NPs, a detailed structural analysis using high magnification SEM images was performed. In figure 4(a) a

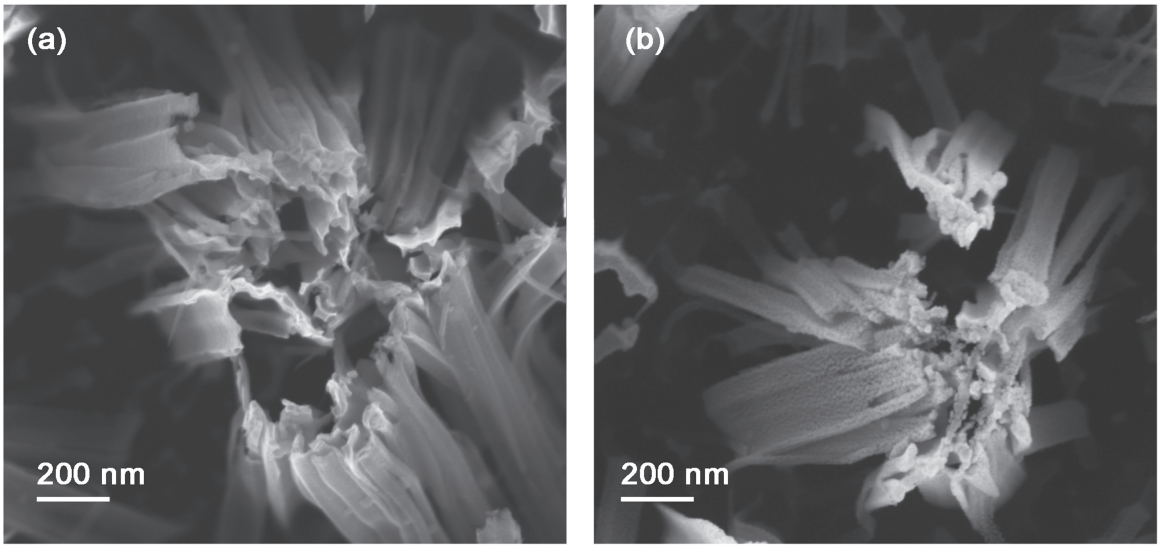

Figure 3. Plan view SEM images of 3.4 μm Si NWs (a) without decoration and (b) decorated by Ag NPs after 60 000 laser pulses.

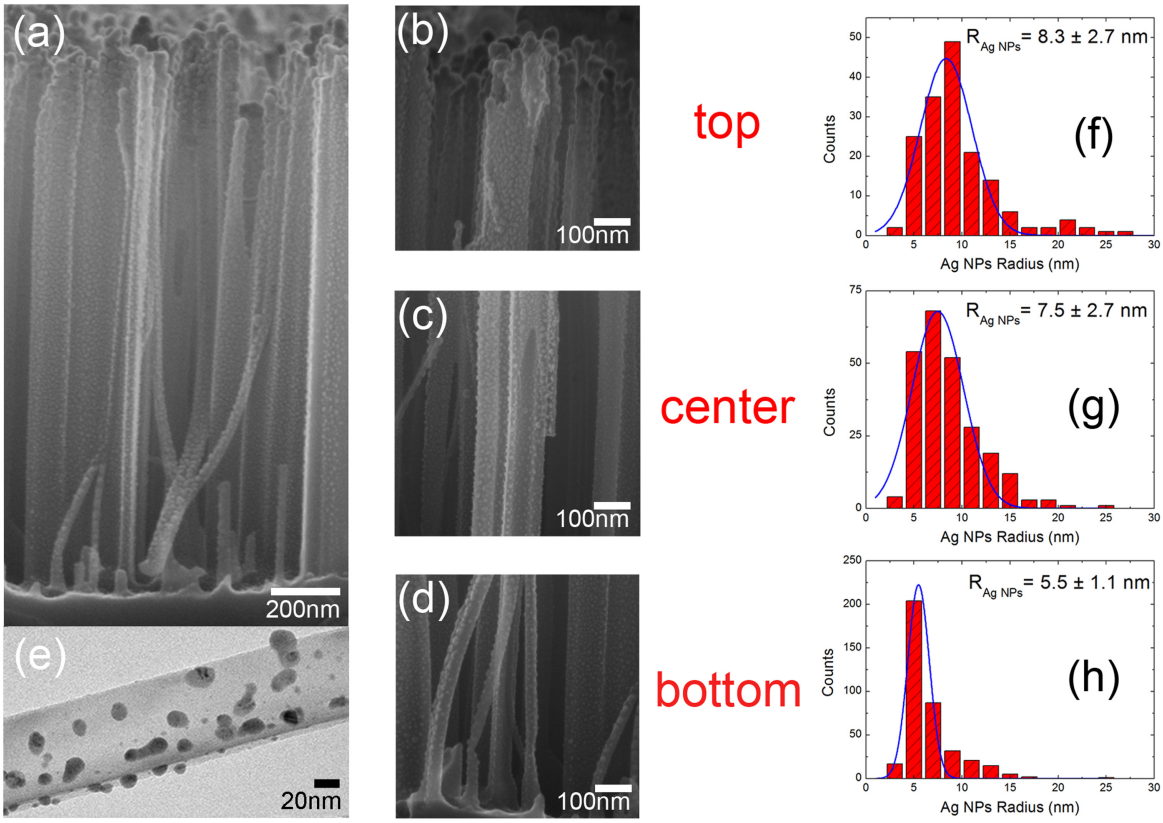

Figure 4. (a) Cross section SEM image of sample 1, high magnification details of the top (b), center (c) and bottom (d) sections of the Si NWs are reported, respectively. In figure (e) a TEM microscopy image of the bottom region of the decorated Si NW is reported. The statistical analysis of the Ag NPs radii is reported for sample 1 associated with the top (f), center (g) and bottom (h), respectively.

cross section SEM image of sample **1** is reported. In figures 4(b)–(d) high magnification SEM cross images of three different sections of the wires are visible, respectively acquired at the top (b), center (c) and bottom part (d) of the decorated NWs. Here, the NP size distributions have been calculated for each different section, the corresponding mean radii and standard deviations were calculated by fitting the size distributions with Gaussian profiles. At the bottom section of the NWs, as reported in figure 4(h), the mean radius of the Ag NPs was estimated at 5.5 ± 1.1 nm. In the central section of the NWs a denser and a more uniform coverage is observed, with larger, but still separated, NPs having a mean radius of 7.5 ± 2.7 nm (g). On the top of the Si NWs the presence of coalesced NPs is clearly visible, forming Ag NPs

Table 2. Statistical results of Ag NP mean radii and first neighbor Ag NP distance along the top, center and bottom sections of the different NW samples. The reported mean values were obtained by fitting the size distributions by Gaussian profiles.

		Sample 1	Sample 2	Sample 3	Sample 4
NW length (μm)		1.7	1.7	3.4	3.4
Laser pulses		45 000	60 000	45 000	60 000
Ag NP mean radius r (nm)	bottom	5.3 ± 1.1	6.9 ± 2.2	4.6 ± 2.5	5.7 ± 1.5
	center	7.5 ± 2.7	7.4 ± 2.2	5.2 ± 2.7	7.6 ± 3.8
	top	8.3 ± 2.7	11.3 ± 4.3	7.3 ± 4.7	10.4 ± 3.0
Ag NP interstitial mean distance g (nm)	bottom	6.5 ± 3.2	6.0 ± 3.0	9.8 ± 6.0	13.6 ± 12.2
	center	5.3 ± 1.9	4.8 ± 1.8	5.1 ± 2.0	11.5 ± 9.4
	top	3.8 ± 1.0	3.0 ± 1.0	4.3 ± 2.0	8.6 ± 4.7

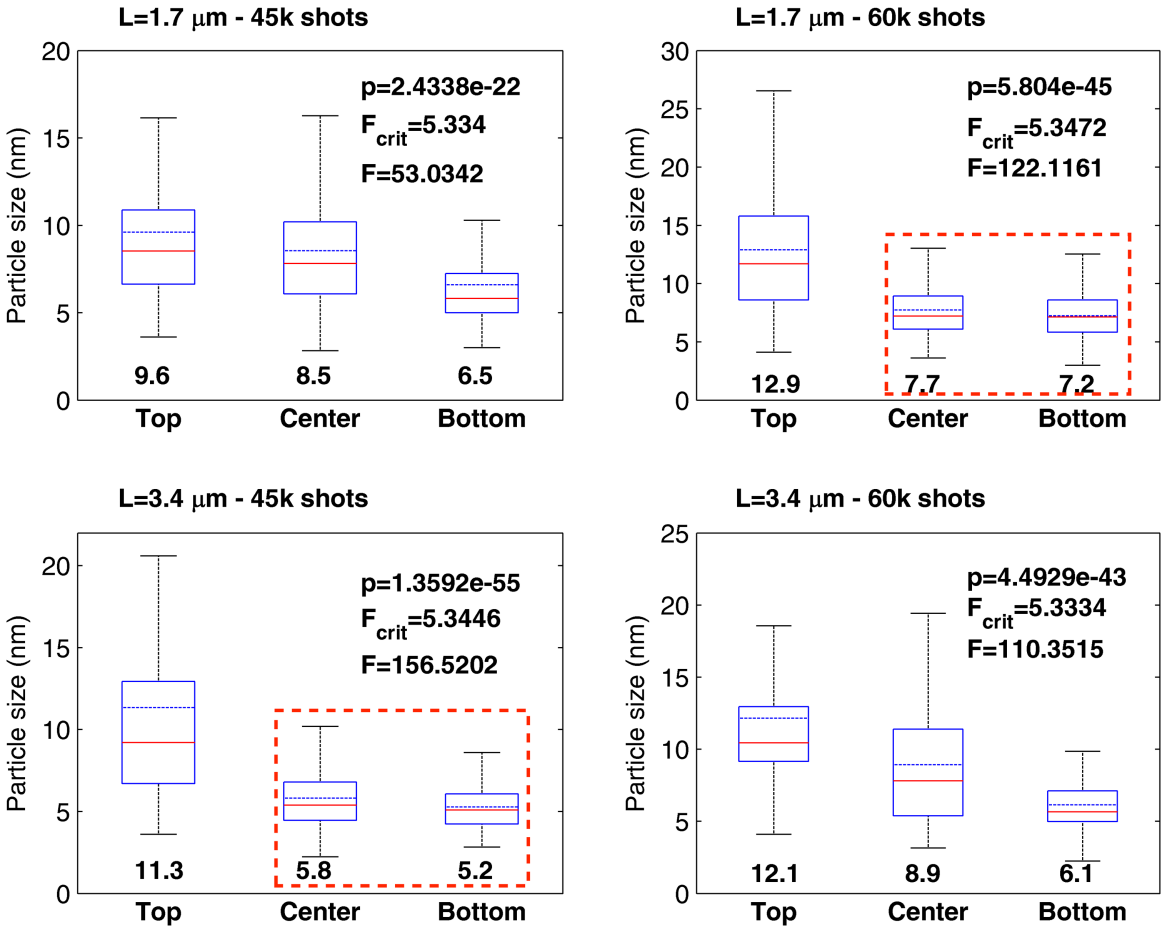

Figure 5. One-way ANOVA results for all the samples. The mean values of the NP size for each groups are reported (corresponding to the dashed blue line). Red lines indicate the median values, upper and lower edges of the boxes represent the 75th and 25th percentile, respectively. The whiskers indicate the interval between the larger and smaller NP sizes not considered as outliers (not shown). The F critical value, calculated at the confidence level of $p = 0.005$, is compared to the ANOVA ones, reported in the figures together with the calculated p values. ANOVA indistinguishable resulted groups are marked by the red dashed boxes (see text).

with a mean radius of 8.3 ± 2.7 nm (f). The dimension of Ag NPs is confirmed by TEM analyses; as an example in figure 4(e) the high resolution TEM image of the bottom region is reported. A mean radius of about 5.2 ± 3.6 nm has been evaluated from TEM analysis, resulting in very good agreement with the statistical study performed on the corresponding SEM image of the same region (figure 3(h)). We performed the same structural study for all samples. Sample **2** obtained by increasing the shot number shows a slight increase of the mean radius. The size of the Ag NPs in the bottom section is 6.9 ± 2.2 nm, in the central section is 7.4 ± 2.2 nm, and at the top is 11.3 ± 4.3 nm. A similar trend has been observed for the longer NWs (samples 3 and 4). Also in this case a good coverage is observed along the

different sections of the NWs and the mean radius of the Ag NPs increases from the bottom to the top as reported in table 2 which summarizes all data.

In summary, for all samples the Ag NP mean size increases from the bottom to the top section of the wires. In order to test further such a conclusion we performed a one-way ANOVA statistical analysis. The NP sizes collected at the different positions along the Si NW length were divided into three groups: top, center and bottom. The ANOVA test was performed to reject the null hypothesis (H_0) i.e. that the means (μ_i, i = 1, 2, 3) of the three groups do not show any significant difference (H_0; $\mu_1 \approx \mu_2 \approx \mu_3$) The results of the ANOVA test are reported in figure 5. The box plots report the mean values for each group (corresponding to the dashed blue line), the median (red line), the 75th and 25th percentile values (upper and lower edges of the box, respectively) and the larger and smaller values not considered as outliers (upper and lower whiskers). As it can be seen the mean valu trend agrees well with the one reported in table 2: the NP sizes decrease going from the top of the NWs to the bottom part. It can be noted also that ANOVA calculated mean values are systematically slightly larger than those reported in table 2. This is not surprising when the way the latter were obtained is considered, i.e. by fitting the size distribution with a Gaussian function, that can underestimate the contribution of the bigger NPs. For each sample the critical F value (F_{crit}) was calculated and corresponds to the degree of freedom between groups ($d_f = 2$) and within groups ($d_{fk} = 791, 578, 610, 804$) at the probability level of $p = 0.005$ (well below the p value of 0.05 usually adopted to validate the null hypothesis) to be compared to the F values resulting from the one-way ANOVA analysis. It can be seen how all the calculated F values are much larger than the corresponding critical ones (see figure 5). At the same time the calculated p values are nearly zero, a result that allows us to safely exclude the null hypothesis, i.e. that *all* the means of the three groups (top, center and bottom) are equal. Nevertheless, such a result cannot rule out the occurrence that two out of three groups could have an equal mean (i.e. $\mu_1 \approx \mu_2 \neq \mu_3$), and, as a consequence, are indistinguishable from a statistical point of view. A multiple comparison procedure, then, was applied to the ANOVA results. The test, performed using both the least significant and Tukey's methods [33, 34] showed that for samples **1** and **4** all three groups have different means, pointing out a different size distribution of the NPs at the top, center and bottom of the Si NWs. For samples **2** and **3** the comparison procedure showed that the NP size distributions for the bottom and center regions (see the values enclosed by the dashed red boxes in figure 5) are equal but significantly different from the one observed at the top.

This evidence can be understood if the NP formation mechanism is considered. In the first stage, NPs form during flight, before reaching the sample. Initially the Ag NPs arrive with the same mean radii on the three different sections of the wires, but since the top of the NWs is more exposed to catch the incident Ag NPs, the formation of coalesced NPs with larger size is more likely. A smaller fraction of the incident NPs reaches the center of the NWs and an even a smaller one can land at the bottom, determining the observed decreasing mean size of the Ag NPs along the wire length from top to bottom, irrespective of the NW length and of the laser shots number. An increment of the NP mean radius is observed when the laser shots number was changed from 45 000 to 60 000. Such a behavior can be easily understood when considering that the number of Ag NPs impinging on the substrate increases, thus it is more likely that small clusters coalesce to form larger NPs. A further critical parameter for applications is the average edge-to-edge distance between Ag NPs. From the same SEM images we measured the mean distance among adjacent NPs for all the samples. All the data gathered from the SEM analysis are shown in table 2. Also for these data the ANOVA procedure was performed, the result indicates that the distance between Ag NPs decreases on going from the bottom to the top of the NWs; even in this case the ANOVA calculated mean values were found to be slightly larger than the ones reported in table 2, but the overall trend was confirmed. The results clearly show how it is possible to change the size distribution, the distance between NPs and the surface coverage in a very simple way just by varying the length of the NWs or the shot number of the PLD process.

3.2. Optical properties

The SERS activity of both decorated and non-decorated samples was checked against the presence of Rhodamine 6G (R6G). For this purpose the samples were soaked in a 10^{-6} M water solution of R6G for 150 min and left to dry in air before Raman measurements.

In figure 6(a) the spectra acquired on the surface of the non-decorated (red line) and decorated (blue line) sample **4** are shown. No Raman signal is detectable in the spectrum acquired on the surface of the bare Si NWs, while the observed broad and intense background is due to the R6G fluorescence. On the other hand, the R6G Raman signatures, superimposed on the fluorescence background, are clearly visible in the spectrum acquired on the surface of the decorated Si NWs (blue line). Subtracting the fluorescence background (black line in figure 6(a)) the most intense R6G vibrational modes, peaked at 618 and related to the C-C-C ring in plane bending, and at 1364, 1513, 1570, 1652 cm^{-1}, relative to C-C symmetric stretching modes, are evident [35].

It is worth noticing that, although the two spectra have been acquired under the same experimental conditions (laser power, objective, slit aperture, acquisition time), the fluorescence intensity in the spectrum recorded from the decorated substrate is ≈1.5 times higher with respect to the fluorescence signal recorded on the surface of the bare Si NWs. The presence of fluorescence originating from the Ag NP decorated surface points to the presence of a certain amount of R6G molecules not adsorbed on the metallic surface, where fluorescence quenching takes place. The observed increase of the fluorescence signal, thus, can be understood if the fluorescence of some of the R6G molecules (not adsorbed on the metallic surface) are enhanced by plasmonic effects that increase the local exciting field [36, 37].

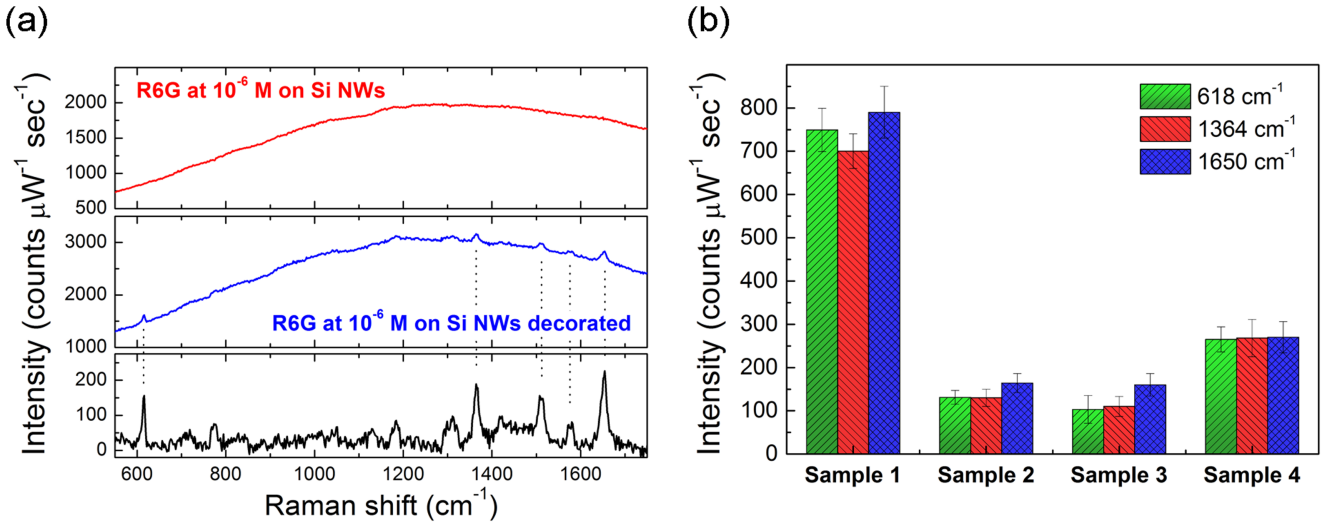

Figure 6. (a) Raman/SERS spectra of Si NWs non-decorated (red line) and Ag decorated (blue line), both immersed in a 10^{-6} M R6G water solution. Due to the Ag NPs the SERS peak relative to the R6G vibrations is clearly detectable and highlighted when the fluorescence background is subtracted (black line). (b) Block diagram reporting the SERS intensities of the R6G Raman modes at 618, 1364 and 1652 cm^{-1} measured on the different Ag decorated Si NWs. The SERS intensities are the average of 10 measures at different sample positions, the error bars are the corresponding intensity standard deviation.

The results of SERS measurements performed on all the decorated samples (from **1** to **4**) are shown in the bar plot in figure 6(b), that reports the intensities of the R6G modes peaked at 618, 1364 and 1652 cm^{-1}, normalized to the power and accumulation time; the fluorescence background was numerically subtracted from all the spectra. Sample **1** performs better than the others, showing a SERS intensity ≈4–5 times higher than sample **2** and sample **3**, and ≈2 times higher than sample **4**.

It is well known that the SERS response of nanostructured surfaces is strongly dependent on their optical properties and notably the strong amplification of the local EM field in the proximity of the nanostructured metallic surface. Such an amplification is due to excitation of localized surface plasmonic resonances (LSPR) of individual NPs or nearby structures optically coupled. Thus an optical characterization of the decorated NWs showing the best SERS performance (samples **1** and **4**) was carried out. In particular, the LSPR behaviour of the Ag NPs was investigated through diffuse reflectance measurements, since transmittance experiments were not achievable due to the non-transparent substrate of the samples. In the diffuse reflectance geometry, the specular component of the light reflected at the sample surface is excluded from the integrating sphere, allowing the measurement of the diffused light only. In order to put in evidence the Ag NP contribution with respect to the optical response of the bare Si NW forest, typically affected by a strong light absorption due to in plane scattering effects, the reflectance spectra were normalized to the diffuse reflectance of the decorated and non-decorated Si NWs, according to

$$I_{\text{Ag NPs}} = I_{\text{NWs decorated}}/I_{\text{NWs bare}} \quad (1)$$

here $I_{\text{NWs decorated}}$ and $I_{\text{NWs bare}}$ are the diffuse reflectance intensities of the decorated and non-decorated Si NWs samples, respectively.

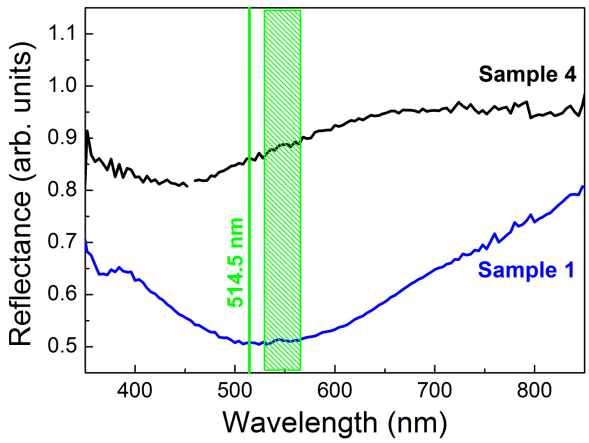

Figure 7. Normalized reflectance spectra showing LSPR spectra of Ag NPs deposited on Si NWs by PLD (sample 1: NWs 1.7 μm long, 45 K shots; sample 4: NWs 3.4 μm long, 60 K shots). The plasmon resonances are obtained following equation (1) by comparing the diffused reflectance spectra of bare and Ag decorated Si NWs. The green line is the laser excitation wavelength, tuned at 514.5 nm, while the green box is the Raman scattering region of the R6G probe molecules (550–1750 cm^{-1}).

Figure 7 shows the normalized reflectance spectra, in the range between 350 and 850 nm, of the decorated Si NWs having the best SERS performances (as visible in figure 6(b)). The spectrum of sample **1** shows a broad minimum of the reflectance signal, that can be identified as a plasmon absorption peak, centred at 540 nm and extending from 400 to 700 nm. A similar behaviour is observed for sample **4** (longer NWs) but in this case the plasmon resonance ranges from 350 to 600 nm and peaks at 450 nm.

The diameter and the average distance of the Ag NPs produced by PLD play a crucial role in terms of LSPR position and thus of SERS efficiency [38]. As reported in

table 2, the increase of the PLD laser shots number allows a larger coalescence among NPs on the NW tops, resulting in an increase of the NP diameter, and a good NP coverage down to the basis in Si NWs. On the other hand, the mean NP distance depends on both the NW length and on the laser shots number, resulting in a different efficiency of optical coupling. Thus, in our set of samples, Ag NPs on sample **1** appear to be optically coupled [39], giving rise to the formation of hot spots and then matching the condition for an optimal SERS efficiency at the excitation wavelength fixed at 514.5 nm. In comparison to sample **1** the variations of the NP mean dimension (sample **2**), of the NP distribution along the NW length (sample **3**) or the interparticle distance (sample **4**), result in a lower SERS efficiency due to a plasmon resonance shift, to lower hot-spots density, or to a less efficient optical coupling between the NPs, respectively. NPs on sample **4**, in particular, show a plasmon resonance typical of a spherical isolated dispersion, and thus weakly coupled [25, 38, 40–42].

The spectra reported in figure 6(a) can be also used to calculate the SERS enhancement factor (EF), typically defined as the ratio between the observed SERS and Raman intensities per molecule. As reported in the literature [38], the normal Raman signal from R6G molecule is not discernible even for samples soaked in Rhodamine aqueous solution at higher concentrations. Thus, the EF was evaluated by comparing the Raman and the fluorescence cross sections, σ_R and σ_F, respectively [38, 43]. In particular, the signal intensities ratio per molecule and per watt power is the ratio between cross sections:

$$\frac{I_{SERS}}{I_F} = EF\frac{I_{Raman}}{I_F} \approx EF\frac{\sigma_{Raman}}{\sigma_F} \approx EF \times 10^{-9} \Rightarrow EF = 10^9\frac{I_{SERS}}{I_F} \quad (2)$$

where I_{SERS} is the SERS intensity for an excitation wavelength at 514.5 nm, and I_F is the intensity of the fluorescence background intensities coming from the decorated substrates. The Raman cross section of R6G is of the order of 10^{-29} cm^2 and it becomes 10^{-25} in resonance conditions ($\lambda_{exc} = 514.5$ nm) [38, 43]. At the same wavelength the fluorescence cross section is about 10^{-16} cm^2 [44, 45]. As a consequence, a factor of about 10^{-9} is expected from the ratio between I_{Raman} and I_F, as indicated in equation (2).

Evaluating the ratio between the averaged normalized intensities for SERS and the respective fluorescence intensity in sample **1** and in sample **4**, EF values of 3×10^8 and 1×10^8, respectively, are obtained. These results demonstrate very good performances of the decorated Si NWs as SERS active substrates.

The EFs, in fact, were one order of magnitude higher with respect to the EF of 1.9×10^7, measured following the same procedure for the highest SERS active substrate made of Ag NPs deposited by PLD on a flat glass surface [38] This result is likely due to the higher number of active hot spots distributed especially along the wires, in a 3D architecture, with respect to the 2D case.

Since one of the most important applications of the SERS active substrates is the development of SERS-based sensors [40, 46], together with the estimation of the SERS EF, we focused attention on evaluating the lower limit of detection achievable with our samples, taken as the smallest detectable concentration of the target analyte. To this purpose, SERS measurements on sample **1** were performed, as a function of the molar concentration of R6G dissolved in an aqueous solutions in the range from 10^{-9} M to 10^{-4} M.

Figure 8(a) shows the averaged SERS spectra as a function of the R6G concentration, acquired at different points on the surface of sample **1** under 514.5 nm excitation. All the spectra have been normalized to the acquisition time and laser power to make possible a direct comparison to each other. Moreover, we should point out that in the shown spectra the fluorescence background has been removed to better compare SERS signals at different concentrations. The R6G SERS signal is clearly visible starting from 10^{-8} M R6G concentration, while no SERS signal is appreciable in the 10^{-9} M spectrum. Indeed, the emission signal from all our samples results from by the overlap of two contributions: the fluorescence broad band and the superimposing SERS peaks. Thus, we can consider the fluorescence signal as noise with respect to the SERS signal. The intensities of three SERS peaks at 618 cm^{-1}, 1364 cm^{-1} and 1650 cm^{-1} have been measured and reported as a function of R6G concentration in figure 6(b). The intensity of the three vibrational modes increases linearly, on a logarithm scale, within the R6G concentration range from 10^{-8} M to 10^{-6} M. Then, the intensities slightly decrease for the 10^{-5} M and 10^{-4} M concentrations. The saturation of the SERS signal at a given concentration is presumably due to the saturation of the SERS active sites by the adsorbed R6G molecules. The slight decrease of the SERS intensity for concentrations above 10^{-6} M can be understood if the behaviour of SERS and fluorescence signals is taken into account. In fact, SERS active substrates can amplify the overall molecular emission signal. The fluorescence background and the SERS are competing emission signals, and as above the 10^{-6} M concentration, the fluorescence background becomes significantly intense, pointing to an increase of the number of non-adsorbed R6G molecules. Since the incoming light is absorbed by such molecules, a reduction of the SERS exciting radiation occurs. For each averaged spectrum we computed the pertinent standard deviation in order to check the uniformity of the SERS signal across the surface. The spot to spot variations were taken into account by calculating the standard deviation for each set of measurements; as an example in the bottom panel of figure 8(b) we report the average spectrum and the standard deviation acquired on the surface of sample **1** after being soaked in a R6G 10^{-5} M solution. The intensity variations of the three peaks used to draw the calibration curve reported in figure 8(b) (top panel) were found to be within 15%, a value that matches the test criteria of reproducibility over a defined area for a SERS substrate: typically better than 20% [47–50].

We comment that the present study addresses the potential of 3D Si NW substrates as SERS sensors, as demonstrated above, while no optimization was performed in order to increase their SERS activity. We believe that there is

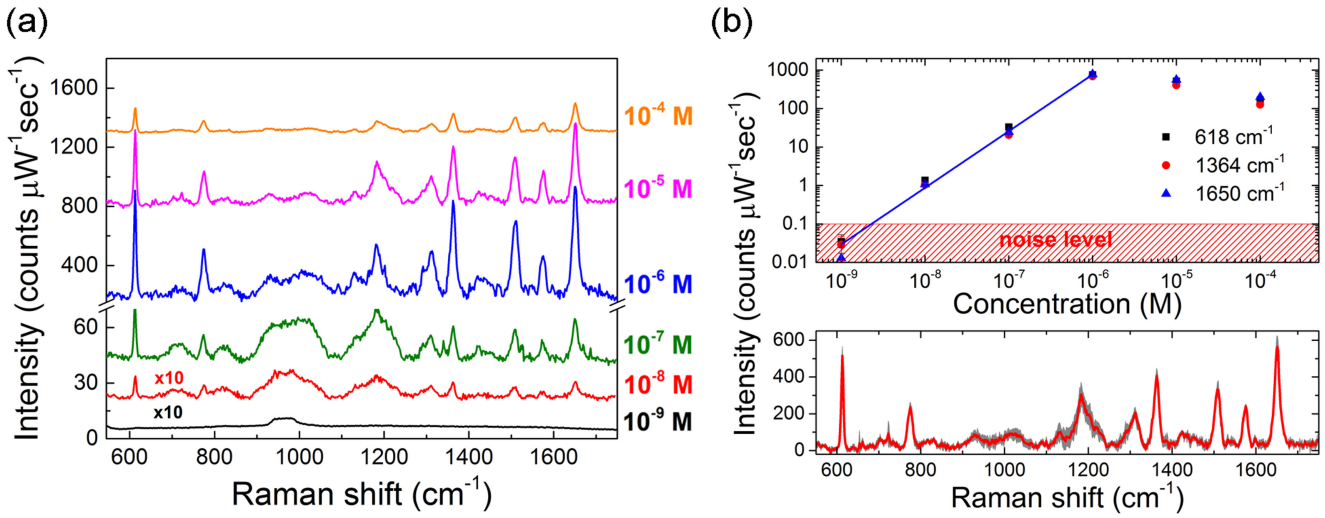

Figure 8. (a) SERS spectra of R6G acquired on sample 1 for different concentrations ranging from 10^{-4} to 10^{-9} M. The fluorescence background was removed for clarity. (b) Top: calibration curve reporting the SERS intensities of the R6G Raman modes (618, 1364, 1652 cm^{-1}) at increasing R6G concentrations from 10^{-9} to 10^{-4} M; bottom: the gray area highlights the SERS intensity standard deviation of the spectra acquired at 10 different positions on the surface of sample **1** soaked in 10^{-5} M R6G solution.

room for optimization of the SERS properties of the substrates, by playing with both the Si NW length and the laser pulses number, in order to increase both the number of SERS active sites and their efficiency.

4. Conclusions

We demonstrated the decoration of silicon nanowires (Si NWs) with silver nanoparticles (Ag NPs) by an industrially compatible method. The pulsed laser deposition (PLD) technique has been extensively discussed as a valid solution to obtain a uniform and dense decoration of Si NW arrays with Ag NPs. Such Si NWs decorated with Ag NPs are chemically shell free and show uniform coverage along the NW length. Moreover, by this room temperature approach we showed a strict control of size, distribution and mutual distance among Ag NPs. We characterized decorated Si NWs as surface enhanced Raman scattering (SERS) active substrates by immersing molecular aqueous solution, using R6G as probe analyte. The SERS spectra clearly reveal the detection power of the decorated substrates characterized by an enhancement factor of the Raman signal higher than 10^8, one order of magnitude above the one of Ag NPs deposited with a similar procedure on a 2D substrate. These results strongly attest to the great potential of a 3D SERS substrate as a powerful sensor for the detection of analytes of practical interest, as was demonstrated in previous works on 2D substrates covered by PLD deposited Ag NPs. On such substrates organic dyes (alizarine, purpurine, brazilin, brazilein, kemesic and carminic acid), of interest in the cultural heritage field, were detected in aqueous solutions at concentration levels down to 10^{-7} M [51].

Acknowledgments

N.C. acknowledges the Italian Project FIRB Futuro in Ricerca 2008 (grant n. RBFR088SW7, funded by MIUR) for partial financial support.

References

[1] Colinge J P *et al* 2010 Nanowire transistors without junctions *Nat. Nanotechnol.* **5** 225

[2] Duan X F, Huang F, Cui X, Wang J F and Lieber C M 2001 Indium phosphide nanowires as building blocks for nanoscale electronic and optoelectronic devices *Nature* **409** 66

[3] Tian B, Zheng X, Kempa T J, Fang Y, Yu N, Yu G, Huang J and Lieber C M 2007 Coaxial silicon nanowires as solar cells and nanoelectronic power sources *Nature* **449** 885

[4] Tsakalakos L, Balch J, Fronheiser J, Korevaar B A, Sulima O and Rand J 2007 Silicon nanowire solar cells *Appl. Phys. Lett.* **91** 233117

[5] Cui Y, Wei Q Q, Park H K and Lieber C M 2001 Nanowire nanosensors for highly sensitive and selective detection of biological and chemical species *Science* **293** 1289

[6] Bunimovich Y L, Shin Y S, Yeo W S, Amori M, Kwong G and Heath J R 2006 Quantitative real-time measurements of DNA hybridization with alkylated nonoxidized silicon nanowires in electrolyte solution *J. Am. Chem. Soc.* **128** 16323–31

[7] Artoni P, Irrera A, Iacona F, Pecora E F, Franzò G and Priolo F 2012 Temperature dependence and aging effects on silicon nanowires photoluminescence *Opt. Express* **20** 1483–90

[8] Priolo F, Gregorkiewicz T, Galli M and Krauss T F 2014 Silicon nanostructures for photonics and photovoltaics *Nat. Nanotechnol.* **49** 19–32

[9] Den Hertog M I, Rouviere J, Dhalluin F, Desré P, Gentile P, Ferret P, Oehler F and Baron T 2008 Control of gold surface diffusion on Si nanowires *Nano Lett.* **8** 1544–50

[10] Lo Faro M J *et al* 2015 Silicon nanowire and carbon nanotube hybrid for room temperature multiwavelength light source *Sci. Rep.* **5** 16753

[11] Fazio B *et al* 2016 Strongly enhanced light trapping in a two-dimensional silicon nanowire random fractal array *Light Sci. Appl.* **5** e16062

[12] Peng K, Xu Y, Wu Y, Yan Y, Lee S T and Zhu J 2005 Aligned single-crystalline Si nanowire arrays for photovoltaic applications *Small* **1** 1062

[13] Peng K, Yan Y, Gao S and Zhu J 2003 Dendrite-assisted growth of silicon nanowires in electroless metal deposition *Adv. Funct. Mater.* **13** 127

[14] Peng K, Wu Y, Fang H, Zhong X Y, Xu Y and Zhu J 2005 Uniform axial-orientation alignment of one-dimensional single-crystal silicon nanostructure arrays *Angew. Chem. Int. Ed. Engl.* **44** 2737

[15] Zhang M L, Peng K Q, Fan X, Jie J S, Zhang R Q, Lee S T and Wong N B 2008 Preparation of large-area uniform silicon nanowires arrays through metal-assisted chemical etching *J. Phys. Chem.* C **112** 4444

[16] Galopin E, Barbillat J, Coffinier Y, Szunerits S, Patriarche G and Boukherroub R 2009 Silicon nanowires coated with silver nanostructures as ultrasensitive interfaces for surface-enhanced Raman spectroscopy *ACS Appl. Mater. Interfaces* **1** 1396–403

[17] Shao M W, Zhang M L, Wong N B, Ma D D, Wang H, Chen W and Lee S T 2008 Ag-modified silicon nanowires substrate for ultrasensitive surface enhanced Raman spectroscopy *Appl. Phys. Lett.* **93** 233118

[18] Zhang M L, Fan X, Zhou H W, Shao M W, Zapien J A, Wong N B and Lee S T 2010 A high-efficiency surface-enhanced Raman scattering substrate based on silicon nanowires array decorated with silver nanoparticles *J. Phys. Chem.* C **114** 1969–75

[19] Fang C, Agarwal A, Widjaja E, Garland M V, Wong S M, Linn L, Khalid N M, Salim S M and Balasubramanian N 2009 Metallization of silicon nanowires and SERS response from a single metallized nanowire *Chem. Mater.* **21** 3542–8

[20] Zhang B, Wang H, Lu L, Ai K, Zhang G and Cheng X 2008 Large-area silver-coated silicon nanowire arrays for molecular sensing using surface-enhanced Raman spectroscopy *Adv. Funct. Mater.* **18** 2348

[21] Yasseri A A, Sharma S, Kamins T I, Li Z and Stanley Williams R 2006 Growth and use of metal nanocrystal assemblies on high-density silicon nanowires formed by chemical vapor deposition *Appl. Phys.* A **82** 659

[22] Jiang Z Y, Jiang X X, Su S, Wei X P, Lee S T and He Y 2012 *Appl. Phys. Lett.* **100** 203104

[23] Zhang M L, Fan X, Zhou H W, Shao M W, Zapien J A, Wong N B and Lee S T 2010 *J. Phys. Chem.* C **114** 1969

[24] Mulazimoglu E, Nogay G, Turan R and Unalan H E 2013 Enhanced localized surface plasmon resonance obtained in two step etched silicon nanowires decorated with silver nanoparticles *Appl. Phys. Lett.* **103** 143124

[25] D'Andrea C, Neri F, Ossi P M, Santo N and Trusso S 2009 The controlled pulsed laser deposition of Ag nanoparticle arrays for surface enhanced Raman scattering *Nanotechnology* **20** 245606

[26] Fazio E, Neri F, Ossi P M, Santo N and Tusso S 2009 Growth process of nanostructured silver films pulsed laser ablated in high-pressure inert gas *Appl. Surf. Sci.* **255** 9676

[27] Patrone L, Nelson D, Safarov V I, Sentis M, Marine W and Giorgio S 2000 Photoluminescence of silicon nanoclusters with reduced size dispersion produced by laser ablation *J. Appl. Phys.* **87** 3829–37

[28] Scuderi D, Albert O, Moreau D, Pronko P P and Etchepare J 2005 Interaction of a laser-produced plume with a second time delayed femtosecond pulse *Appl. Phys. Lett.* **86** 071502

[29] Neri F, Ossi P M and Trusso S 2011 Cluster synthesis and assembling in laser generated plasma *La Rivista Nuovo Cimento* **34** 103

[30] Micali N, Neri F, Ossi P M and Trusso S 2013 Light scattering enhancement in nanostructured silver film composites *J. Phys. Chem.* C **117** 3497–502

[31] Lu R, Sha J, Xia W, Fang Y, Gu L and Wang Y 2013 A 3D-SERS substrate with high stability:silicon nanowire arrays decorated by silver nanoparticles *Cryst. Eng. Comm.* **15** 6207

[32] Fazio E, Neri F, Ossi P M, Santo N and Trusso S 2009 Ag nanocluster synthesis by laser ablation in Ar atmosphere: a plume dynamics analysis *Laser Part. Beams* **27** 281

[33] Hayter A J 1986 The maximum familywise error rate of Fisher's least significant difference test *J. Am. Stat. Assoc.* **81** 1000

[34] Tukey J 1949 Comparing individual means in the analysis of variance *Biometrics* **5** 99

[35] Yang Y and Meng G 2010 Ag dendritic nanostructures for rapid detection of polychlorinated biphenyls based on surface-enhanced Raman scattering effect *J. Appl. Phys.* **107** 044315

[36] Kinkhabwala A, Yu Z, Fan S, Avlasevich Y, Müllen K and Moerner W E 2009 Large single-molecule fluorescence enhancements produced by a bowtie nanoantenna *Nat. Photon.* **3** 654–7

[37] Farahani J N, Pohl D W, Eisler H J and Hecht B 2005 Single quantum dot coupled to a scanning optical antenna: a tunable superemitter *Phys. Rev. Lett.* **95** 017402

[38] Fazio E, Neri F, D'Andrea C, Ossi P M, Santo N and Trusso S 2011 SERS activity of pulsed laser ablated silver thin films with controlled nanostructure *J. Raman Spectrosc.* **42** 1298

[39] Romero I, Aizpurua J, Bryant G W and García de Abajo F J 2006 Plasmons in nearly touching metallic nanoparticles: singular response in the limit of touching dimers *Opt. Express* **14** 9988–99

[40] Foti A, D'Andrea C, Bonaccorso F, Lanza M, Calogero G, Messina E, Maragò O M, Fazio B and Gucciardi P G 2013 A shape-engineered surface-enhanced Raman scattering optical fiber sensor working from the visible to the near-infrared *Plasmonics* **8** 13–23

[41] Le Ru E C and Etchegoin P G 2007 *Principles of Surface Enhanced Raman Scattering* (Amsterdam: Elsevier)

[42] Kreibig U and Vollmer M 1995 *Optical Properties of Metal Clusters* (Berlin: Springer)

[43] Nie S and Emory S R 1997 Probing single molecules and single nanoparticles by surface-enhanced Raman scattering *Science* **275** 1102

[44] Hildebrandt P and Stockenburger M 1984 Surface-enhanced resonance Raman spectroscopy of rhodamine 6G adsorbed on colloidal silver *J. Phys. Chem.* **88** 5935–44

[45] Kneipp K, Wang Y, Kneipp H, Itzkan I, Dasari R R and Feld M S 1996 Population pumping of excited vibrational states by spontaneous surface-enhanced Raman scattering *Phys. Rev. Lett.* **76** 2444

[46] Cottat M *et al* 2015 High sensitivity, high selectivity SERS detection of MnSOD using optical nanoantennas functionalized with aptamers *J. Phys. Chem.* C **119** 15532–40

[47] Shalaev V M 1996 Electromagnetic properties of small-particle composites *Phys. Rep.* **272** 61

[48] Yang X, Zhong H, Zhu Y, Shen J and Li C 2013 Ultrasensitive and recyclable SERS substrare based on Au-decorated Si nanowire arrays *Dalton Trans.* **42** 14324

[49] Jiang Z Y, Jiang X X, Su S, Wei X P, Lee S T and He Y 2012 Silicon-based reproducible and active surface-enhanced Raman scattering substrates for sensitive, specific, and multiplex DNA detection *Appl. Phys. Lett.* **2012** 203104

[50] Xu Z, Jiang J, Wang X, Han K, Ameen A, Khan I, Chang T W and Liu G L 2016 Large-area, uniform and low-cost dual-mode plasmonic naked-eye colorimetry and SERS sensor with handheld Raman spectrometer *Nanoscale* **8** 6162

[51] Fazio E, Neri F, Valenti A, Ossi P M, Trusso S and Ponterio R C 2013 Raman spectroscopy of organic dyes adsorbed on pulsed laser deposited silver thin films *Appl. Surf. Sci.* **278** 259